PTEP

Prog. Theor. Exp. Phys. **2022** 12B103(22 pages)
DOI: 10.1093/ptep/ptac039

IYBSSD2022
International Year
of Basic Sciences
for Sustainable Development

History of solar neutrino observations

Masayuki Nakahata[1,2]

[1]*Kamioka Observatory, Institute for Cosmic Ray Research, University of Tokyo, 456 Higashi-Mozumi, Kamioka-cho, Hida-shi, Gifu 506-1205, Japan*
[2]*Kavli Institute for the Physics and Mathematics of the Universe (WPI), The University of Tokyo Institutes for Advanced Study, University of Tokyo, Kashiwa, Chiba 277-8583, Japan*
E-mail: nakahata@suketto.icrr.u-tokyo.ac.jp

Received January 15, 2022; Revised February 19, 2022; Accepted March 3, 2022; Published March 7, 2022

The first solar neutrino experiment, led by Raymond Davis Jr, showed a deficit of neutrinos relative to the solar model prediction, referred to as the "solar neutrino problem" since the 1970s. The Kamiokande experiment, led by Masatoshi Koshiba, successfully observed solar neutrinos, as first reported in 1989. The observed flux of solar neutrinos was almost half the predicted value and confirmed the solar neutrino problem. This problem was not resolved for some time due to possible uncertainties in the solar model. In 2001, it was discovered that the solar neutrino problem is due to neutrino oscillations by comparing the Super-Kamiokande and Sudbury Neutrino Observatory results; this was the first model-independent comparison. Detailed studies of solar neutrino oscillations have since been performed, and the results of solar neutrino experiments are consistent with solar model predictions when the effects of neutrino oscillations are taken into account. In this article, the history of solar neutrino observations is reviewed with the contributions of Kamiokande and Super-Kamiokande detailed.

Subject Index C43, F21

1. Introduction

The main energy source of the Sun is thermonuclear reactions inside the core. Considerable amounts of electron-type neutrinos (ν_e) are produced through nuclear fusion reactions, and solar neutrino experiments provide direct surveys of the deep interior of the Sun. Prof. R. Davis established the Homestake experiment to identify the main fusion reactions in the 1960s. However, the observed flux was much smaller than that predicted by the standard solar model, and this was referred to as the "solar neutrino problem". The Homestake experiment used a radiochemical method that collected argon atoms produced by neutrino reactions. Because of the unconventional technique of the experiment, it was unclear whether the solar neutrino problem could be attributed to the properties of neutrinos themselves or whether there were errors in the standard solar model.

The Kamiokande experiment was undertaken in 1983 under the leadership of Prof. Masatoshi Koshiba. The original purpose of Kamiokande was to search for proton decay. Proton decays were not observed and Prof. Koshiba proposed upgrading the detector for solar neu-

© The Author(s) 2022. Published by Oxford University Press on behalf of the Physical Society of Japan. This is an Open Access article distributed under the terms of the Creative Commons Attribution License (https://creativecommons.org/licenses/by/4.0/), which permits unrestricted reuse, distribution, and reproduction in any medium, provided the original work is properly cited.
Funded by SCOAP[3]. SCOAP3 and OUP support the goals of the International Year of Basic Sciences for Sustainable Development

Downloaded from https://academic.oup.com/ptep/article/2022/12/12B103/6543725 by Deutsches Elektronen Synchrotron user on 25 January 2023

trino measurements a few months after data collection was started. In 1988, the Kamiokande experiment succeeded in observing solar neutrinos. This was the first measurement with a real-time detection method. The observed solar neutrino flux was about 50% of the prediction and confirmed the solar neutrino problem. Although the Homestake and Kamiokande experiments observed a deficit in the solar neutrino flux, they could not determine the cause of the discrepancy because of large uncertainties in the model predictions.

In the early 1990s, gallium experiments (SAGE and GALLEX) were started to measure low-energy solar neutrinos. These experiments also observed a flux smaller than the prediction, increasing the possibility of neutrino oscillations being the solution to the solar neutrino problem.

In 1996, Super-Kamiokande, which had 30 times larger fiducial volume than Kamiokande, started collecting data. It had detected about 22 400 solar neutrino events by 2001 and the ^{8}B solar neutrino flux was measured with an accuracy of 3% using neutrino–electron scattering. In 2001, the Sudbury Neutrino Observatory (SNO) group announced a ^{8}B flux measurement using charged-current neutrino–deuteron interactions, and comparisons between the Super-Kamiokande and SNO results gave direct evidence for model-independent solar neutrino oscillations. The evidence was further strengthened by neutral-current measurements from SNO. In 2002, combining the results of the solar neutrino experiments, global analyses showed that the most suitable oscillation parameter is the large mixing angle (LMA; a solution with a mass-squared difference $\Delta m^2_{21} (= m^2_2 - m^2_1)$ of 10^{-5}–10^{-4} eV^2 and a mixing angle (θ) of $\sin^2(2\theta) = 0.5$–1)[1]. In 2008, the Borexino experiment measured the flux of ^{7}Be solar neutrinos and further confirmed the existence of neutrino oscillations.

In this article, results from solar neutrino experiments are reviewed with detailed descriptions of Kamiokande and Super-Kamiokande. In Sect. 2, the standard solar model and its neutrino flux predictions are described. The results of the Homestake experiment are described in Sect. 3 and the observations from Kamiokande are described in Sect. 4. In Sect. 5, the status of our understanding of the solar neutrino problem just before the start of Super-Kamiokande and SNO is summarized, including results from the SAGE and GALLEX experiments. Solar neutrino measurements by Super-Kamiokande, SNO, and Borexino are described in Sects. 6, 7, and 8, respectively. Solar neutrino oscillations are discussed in Sect. 9 and the conclusion and some future prospects are given in Sect. 10.

2. Standard solar model

It is important to develop precise standard solar models in order to discuss neutrino oscillations. In the standard solar model (SSM) [1–3], the time evolution of the temperature and pressure at each position in the Sun is solved using equations of hydrostatic equilibrium, mass continuity, energy conservation, and energy transport by radiation or convection. The boundary conditions for solving the model are the mass, radius, age, and luminosity of the Sun at present. The input parameters for the SSM include nuclear fusion cross sections, the initial chemical composition of the Sun (elements other than H and He), and the opacity to photons. The SSM assumes that the current surface chemical composition reflects the initial chemical composition, and photospectroscopic measurements of the surface are used to estimate its chemical composition.

[1] Details of the oscillation parameters will be described in Sects. 5 and 9.

Downloaded from https://academic.oup.com/ptep/article/2022/12/12B103/6543725 by Deutsches Elektronen Synchrotron user on 25 January 2023

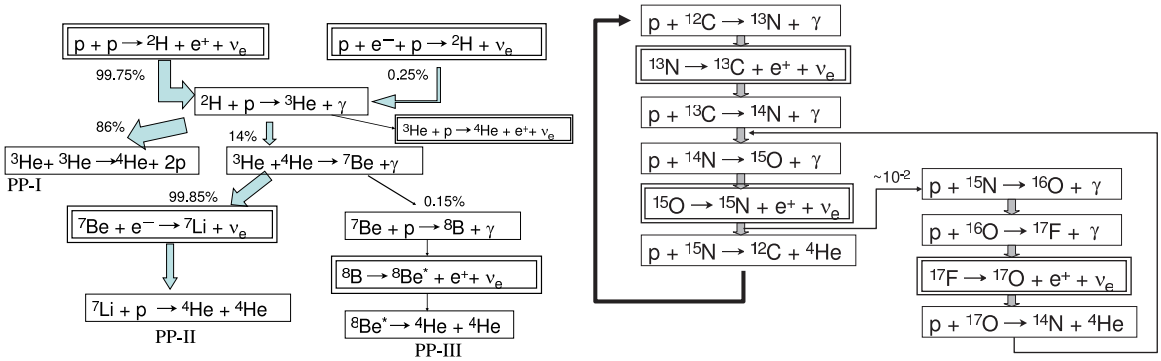

Fig. 1. *pp* chain and CNO cycle reactions.

Table 1. Solar neutrino flux predicted by the SSM [3]. The second and third columns show the flux predictions using the chemical composition from GS98 [4] and AGSS09met [5], respectively.

Source	Flux (/cm^2/s)	
	GS98	AGSS09met
pp	5.98×10^{10} (1 ± 0.006)	6.03×10^{10} (1 ± 0.005)
^{7}Be	4.93×10^{9} (1 ± 0.06)	4.50×10^{9} (1 ± 0.06)
pep	1.44×10^{8} (1 ± 0.01)	1.46×10^{8} (1 ± 0.009)
^{8}B	5.46×10^{6} (1 ± 0.12)	4.50×10^{6} (1 ± 0.12)
hep	7.98×10^{3} (1 ± 0.30)	8.25×10^{3} (1 ± 0.30)
^{13}N	2.78×10^{8} (1 ± 0.15)	2.04×10^{8} (1 ± 0.14)
^{15}O	2.05×10^{8} (1 ± 0.17)	1.44×10^{8} (1 ± 0.16)
^{17}F	5.29×10^{6} (1 ± 0.20)	3.26×10^{6} (1 ± 0.18)

The SSM predicts that 99% of the energy production in the Sun is due to the *pp* nuclear reaction chain and the remaining 1% is due to the CNO cycle, as shown in Fig. 1. In the figure, the reactions marked with double borders produce neutrinos, and the neutrinos from these reactions are named depending on the reaction: *pp*, ^{7}Be, ^{8}B, *hep*, ^{13}N, ^{15}O, and ^{17}F neutrinos. The fluxes of each neutrino type from the latest SSM [3] are shown in Table 1. The second and third columns in the table show the flux predictions using chemical compositions obtained by GS98 [4] and AGSS09met [5], respectively. GS98 is based on a 1D model of the solar atmosphere that was released in 1998. AGSS09met, released in 2009, is based on a 3D model and uses the most up-to-date atomic and molecular data, and should therefore be more reliable than the GS98-based solar model. However, the GS98-based solar model can reproduce various observations inside the Sun, such as the sound speed profile, the depth of the convective zone, and the helium abundance, while the AGSS09met-based solar model's predictions have large discrepancies with observations. Therefore, the flux predictions of both are given here.

The energy spectrum of solar neutrinos predicted by the SSM is shown in Fig. 2. The most energetic neutrino is the ^{8}B neutrino and it was the main neutrino source for the Homestake, Kamiokande, Super-Kamiokande, and SNO experiments, though its intensity is only about 0.01% of the total solar neutrino flux. The most abundant source is the *pp* neutrino but its maximum energy is only 0.42 MeV. The gallium experiments were sensitive to *pp* neutrinos.

Downloaded from https://academic.oup.com/ptep/article/2022/12/12B103/6543725 by Deutsches Elektronen Synchrotron user on 25 January 2023

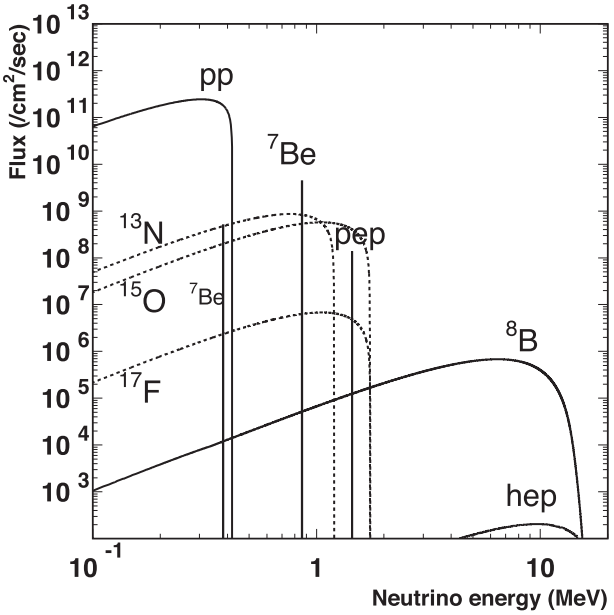

Fig. 2. Solar neutrino energy spectrum expected from the SSM [1,2]. The solid and dashed curves show neutrinos in the *pp* chain and CNO cycle, respectively.

3. Homestake experiment

The Homestake experiment was located in the Homestake goldmine at a depth of 1480 m [6]. The experiment was started around 1970 and data were obtained until 1994. The target for the solar neutrinos was ^{37}Cl atoms in 615 tons of C_2Cl_4. The neutrino energy threshold of the reaction $^{37}\mathrm{Cl} + \nu_e \rightarrow {}^{37}\mathrm{Ar} + e^-$ is 0.814 MeV and it is mainly sensitive to ^{8}B neutrinos. This radiochemical Cl-Ar method of solar neutrino detection was proposed by B. Pontecorvo in 1946 [7]. The expected event rate from the SSM [2] was 8.5±1.8 SNU, where one SNU is 10^{-36} captures/atom/s. The contribution from each neutrino source is 6.6 SNU from ^{8}B neutrinos, 1.2 SNU from ^{7}Be neutrinos, 0.22 SNU from *pep* neutrinos, and the remainder from CNO cycle neutrinos. The produced ^{37}Ar atoms were collected once every 60–120 days and the decay of ^{37}Ar was counted using a low background proportional counter. Figure 3 shows the observed production rate of ^{37}Ar in each collection cycle [6]. The average event rate observed by the Homestake experiment was

$$\phi(\text{Homestake}) = 2.56 \pm 0.16(\text{stat.}) \pm 0.16(\text{sys.})\ \text{SNU}.$$

The observed event rate was only about 30% of the SSM prediction, leading to the so-called solar neutrino problem.

4. Kamiokande

The Kamiokande detector was constructed in 1983 to search for proton decay. The detector had a 2340 ton water volume, located 1000 m underground in the Kamioka mine in Japan. The water volume was viewed by 1000 20-inch diameter photomultipliers (PMTs) mounted on a 1-m grid on the inner surface. Data collection was started on July 6, 1983 and tens of proton decay events within a few months were expected if the original idea of the grand unified theory [8] was correct. However, no proton decay events were found. Since the primary purpose of the detector was to observe events with ∼1 GeV total energy, low-energy events such as solar

Downloaded from https://academic.oup.com/ptep/article/2022/12/12B103/6543725 by Deutsches Elektronen Synchrotron user on 25 January 2023

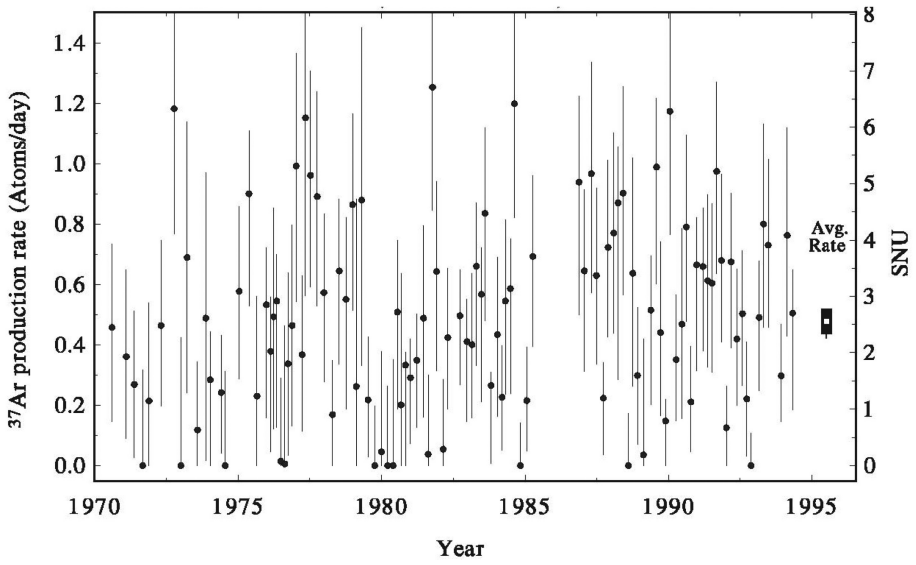

Fig. 3. Data from the Homestake experiment [6]. Each data point shows the ^{37}Ar production rate measured in each collection cycle (run). The scale on the right-hand side is in SNU. The time-averaged rate is shown to the right of the main data.

neutrinos were not triggered in the first stage of the Kamiokande experiment as the electronics at that time read out only the integrated charge information for each PMT. The total sum signal, which is the sum of the analog signals from all PMTs, was used to trigger the readout electronics, and the trigger energy threshold was about 30 MeV for electrons, which is much higher than the energy of solar neutrino signals. The total sum signal was recorded by a transient digitizer (R7912, Tektronix), which records a digitized oscilloscope image in order to detect $\mu \to e$ decay signals from stopping muons. There were several hundred cosmic ray stopping muons per day in the Kamiokande detector. Figure 4 shows the pulse height distribution of $\mu \to e$ signals. The distribution showed that the Kamioka detector had the potential to detect low-energy neutrinos down to $\sim$10 MeV, and Prof. Koshiba proposed upgrading the detector for ^{8}B solar neutrino measurements in the fall of 1983.

In order to detect solar neutrinos, two major upgrades were required. First, an anti-counter system had to be constructed to reduce environmental background signals such as gamma rays from radioactivity in the surrounding rock. Second, a new set of electronics to read out the timing and charge information of each individual PMT was necessary. Precise determination of the position where an event occurred, called the vertex position, is crucial for solar neutrino measurements. The gamma rays from the rock that remained after passing through the anti-counter tended to have a vertex position near the wall of the detector. High-energy cosmic rays produce hadronic cascade showers by spallation and generate short-life radioactive nuclei. The event rate of the beta decays of those nuclei was more than one order of magnitude higher than the expected rate of ^{8}B solar neutrino signals. These spallation products were produced along the track of the originating cosmic ray muons and could be removed using the vertex information.

The anti-counter was constructed from September 1984 to March 1985. 123 20-inch PMTs were mounted in the anti-counter to work as an active veto. The bottom PMT plane of the inner counter was lifted by 1.2 m to allow PMTs to be inserted for the bottom anti-counter.

Downloaded from https://academic.oup.com/ptep/article/2022/12/12B103/6543725 by Deutsches Elektronen Synchrotron user on 25 January 2023

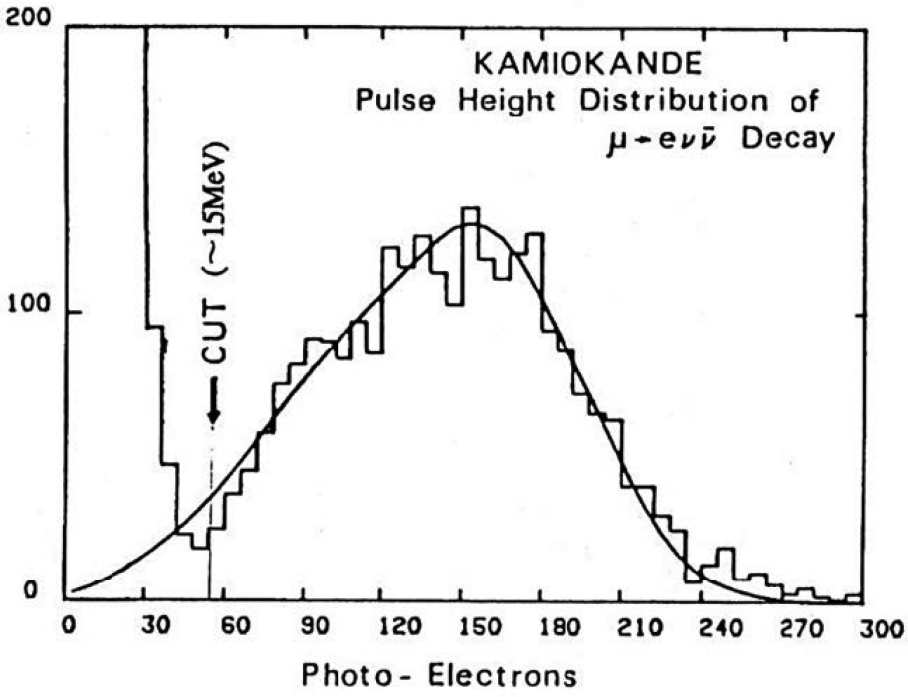

Fig. 4. Pulse height distribution of $\mu \to e$ signals of stopping cosmic ray muons at the early stage of Kamiokande.

The PMTs for the top anti-counter were mounted 0.8 m above the top inner counter. Additional water was added to the tank to submerge these PMTs. The Kamiokande tank was constructed in a newly excavated cavern, and rubber asphalt was sprayed on the surface of the cavern to make it watertight so that water could be added between the cavern wall and the Kamiokande tank. PMTs were mounted in this newly prepared layer, which functioned as the barrel part of the anti-counter. A schematic view of the Kamiokande detector after the upgrade is shown in Fig. 5.

Prof. Koshiba gave a talk on the possibility of detecting ^{8}B solar neutrinos at Kamiokande at ICOBAN'84 (International Conference On BAryon Non-conservation, Park City, Utah, 1984) and asked the participants to collaborate on the electronics upgrade. Soon after this workshop, the University of Pennsylvania group led by Prof. A. K. Mann expressed interest in producing the new electronics. The electronics system, included timing and charge readouts and a trigger system using number-of-hit PMTs, was installed in the fall of 1985.

A further consideration was radon in the tank water, which is the most significant source of background noise in solar neutrino measurements. The concentration of radon, especially ^{222}Rn, was two or more orders of magnitude higher in the air and water in the mine than in the usual environment outside the mine. A daughter of ^{222}Rn, ^{214}Bi, emits beta rays with an end-point energy of 3.27 MeV, which mimics a solar neutrino signal. When Kamiokande started collecting data after the installation of anti-counters, fresh water was being constantly supplied to the tank. The trigger rate in the lower-energy threshold mode was several hundred events per second, while the goal was at most only about one solar neutrino event per day. Figure 6 shows the change in trigger rate after a modification was made to recirculate water rather than supplying fresh water. The decrease in the trigger rate was consistent with the decay of ^{222}Rn with a half life of 3.8 days. Various efforts were made to further reduce radon in the tank water

Downloaded from https://academic.oup.com/ptep/article/2022/12/12B103/6543725 by Deutsches Elektronen Synchrotron user on 25 January 2023

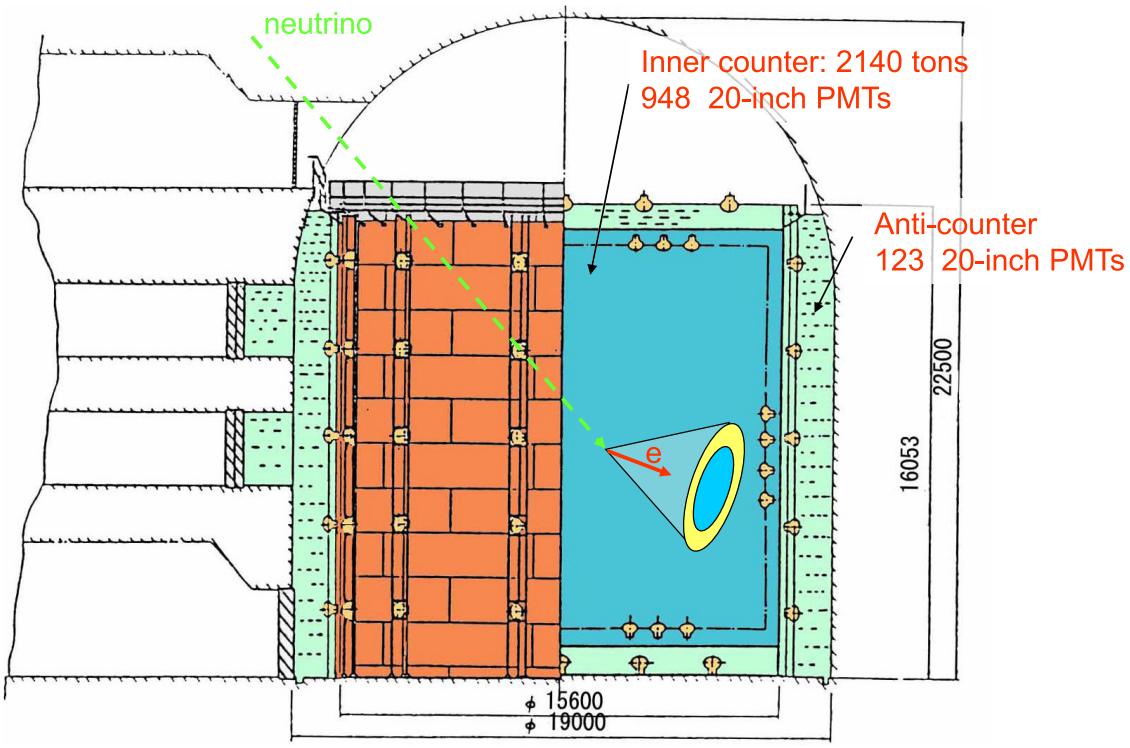

Fig. 5. Schematic view of the Kamiokande detector after the upgrade.

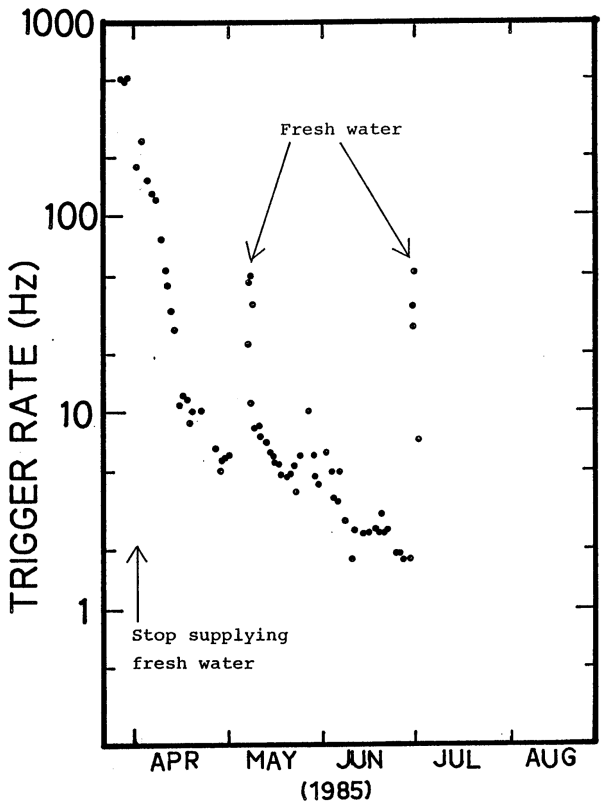

Fig. 6. Change in trigger rate after changing to recirculated water without supplying fresh water.

Downloaded from https://academic.oup.com/ptep/article/2022/12/12B103/6543725 by Deutsches Elektronen Synchrotron user on 25 January 2023

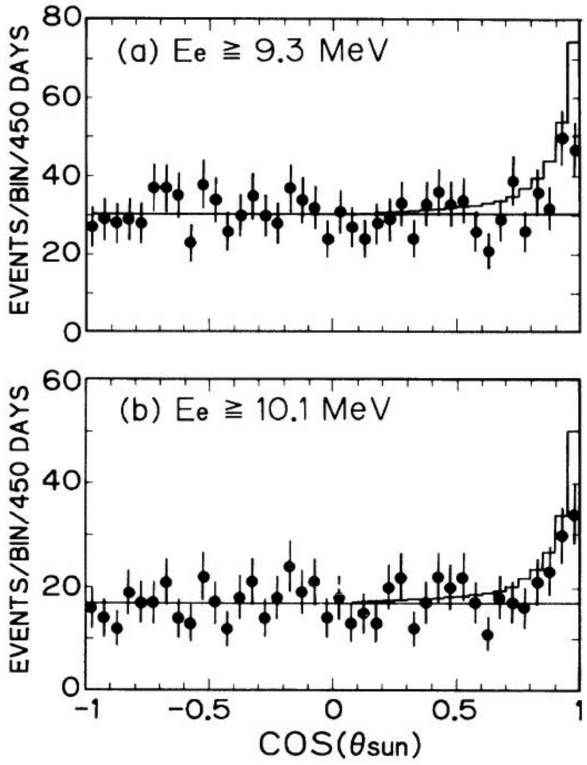

Fig. 7. Angular distribution in the direction of the Sun at Kamiokande [9]. The plot shows data from the first 450 days of data taken from January 1987 to May 1988. The solid histogram shows the prediction from the SSM.

in 1986, including air-tightening of buffer tanks in the water purification system. The detector was almost ready for solar neutrino measurements in early 1987.

Prof. Koshiba noted that the following three features are necessary to perform "neutrino astronomy":

- Directionality
- Real-time measurement
- Energy spectrum measurement

In Kamiokande, solar neutrino signals were observed based on the Cherenkov radiation of recoil electrons from neutrino–electron scattering. Since the energy of the ^{8}B solar neutrino is much larger than the mass of an electron, the direction of a scattered electron is strongly correlated with the direction from the Sun to the Earth. In addition, since Kamiokande observed images of the Cherenkov ring pattern, the direction of the electron could be observed. Kamiokande was a real-time detector and events were observed at the time when they happened. The energy spectrum of the neutrinos could be deduced from the spectrum of the scattered electrons. Thus, the observations at Kamiokande satisfied the criteria for neutrino astronomy.

Figure 7 shows the angular distribution to the Sun for the events that passed the criteria for solar neutrino event selection. The plot was obtained with initial 450-day data taken from January 1987 to May 1988 [9]. A clear excess of events was observed in the direction of the Sun but the observed rate was about 50% of the prediction from the SSM (solid histogram in the figure). This observation confirmed the solar neutrino problem.

Downloaded from https://academic.oup.com/ptep/article/2022/12/12B103/6543725 by Deutsches Elektronen Synchrotron user on 25 January 2023

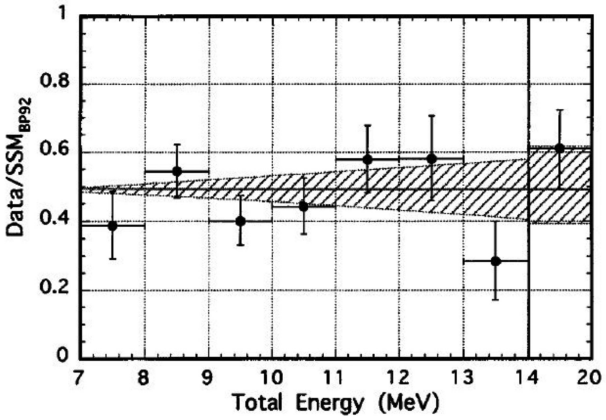

Fig. 8. Energy spectrum of recoil electrons normalized by the predicted spectrum from the 2079-day dataset of Kamiokande. The hatched area shows the range of systematic uncertainty.

The Kamiokande detector had observed ∼600 solar neutrino events by February 1995 [10] and the obtained flux of ^{8}B neutrinos was

$$\phi(^8\mathrm{B})_{\mathrm{Kamiokande}} = 2.80 \pm 0.19(\mathrm{stat.}) \pm 0.33(\mathrm{sys.}) \times 10^6/\mathrm{cm}^2/\mathrm{s}\,.$$

The observed flux was 48±3(stat.)±6(sys.)% of the prediction from the SSM. The energy spectrum of recoil electrons normalized by the predicted spectrum is shown in Fig. 8, consistent with a flat spectrum; i.e., no hint of neutrino oscillations was given in the spectrum. In order to proceed to investigate the possibility of neutrino oscillations, high statistics measurements with Super-Kamiokande were necessary.

5. Status just before the start of Super-Kamiokande and SNO

This section describes other experiments that have been performed and how we enhanced our understanding of the solar neutrino problem before the Super-Kamiokande/SNO era.

SAGE and GALLEX were radiochemical experiments using gallium targets conducted since the early 1990s. The SAGE experiment [11–13] was conducted at the Baksan Observatory and the GALLEX experiment [14–16] (later changed to GNO [17]) was conducted at the Gran Sasso Laboratory. The energy threshold of the gallium reaction ($^{71}\mathrm{Ga} + \nu_e \rightarrow {}^{71}\mathrm{Ge} + e^-$) is 0.233 MeV and is mainly sensitive to low-energy solar neutrinos. The expected event rate from the SSM [2] is 131^{+12}_{-10} SNU, with contributions of 69.6 SNU from *pp* neutrinos, 34.8 SNU from ^{7}Be neutrinos, 13.9 SNU from ^{8}B neutrinos, 2.9 SNU from *pep* neutrinos, and the remainder from CNO cycle neutrinos. SAGE used 50 tons of gallium in metallic form and GALLEX/GNO used 30 tons of gallium in a $GaCl_3$ ·HCl solution. The lifetime of ^{71}Ge is 16.5 days and a typical exposure time for one run was 28 days. By the middle of the 1990s, a deficit of solar neutrinos had been observed at SAGE and GALLEX, where the predicted event rate was mainly coming from robust sources such as *pp* and ^{7}Be neutrinos. The final results of the gallium experiments are shown here but the conclusion has not changed since the middle of the 1990s. The average

Downloaded from https://academic.oup.com/ptep/article/2022/12/12B103/6543725 by Deutsches Elektronen Synchrotron user on 25 January 2023

event rates observed by SAGE and GALLEX/GNO were

$$\phi(\text{SAGE}) = 65.4^{+3.1}_{-3.0}(\text{stat.})^{+2.6}_{-2.8}(\text{sys.})\ \text{SNU}$$
$$\phi(\text{GALLEX}) = 73.1^{+6.1}_{-6.0}(\text{stat.})^{+3.7}_{-4.1}(\text{sys.})\ \text{SNU}$$
$$\phi(\text{GNO}) = 62.9^{+5.5}_{-5.3}(\text{stat.})^{+2.5}_{-2.5}(\text{sys.})\ \text{SNU}.$$

Combining these results [13], the flux measured by the gallium experiments was

$$\phi(\text{gallium}) = 66.1 \pm 3.1\ \text{SNU}.$$

The observed flux is 50% of the expectation from the SSM [2].

Since it was difficult to attribute the deficits of the neutrino event rates at the Homestake, Kamiokande, and SAGE/GALLEX experiments to potential problems in the SSM, the possibility of solar neutrino oscillations was extensively discussed in the mid-1990s. Assuming two types of neutrinos, the relation between the mass eigenstates of the two neutrinos (ν_1 and ν_2) and their interaction eigenstates (ν_e and ν_X (X=μ, τ)) is expressed as

$$\begin{pmatrix} \nu_e \\ \nu_X \end{pmatrix} = \begin{pmatrix} \cos\theta & \sin\theta \\ -\sin\theta & \cos\theta \end{pmatrix} \begin{pmatrix} \nu_1 \\ \nu_2 \end{pmatrix},$$

where θ is the mixing angle. Solving the time evolution of the neutrino wave function, the probability that produced electron-type neutrinos are observed as electron-type neutrinos is

$$P(\nu_e \to \nu_e) = 1 - \sin^2 2\theta \times \sin^2\left(1.27 \times \Delta m^2 \frac{L}{E}\right),$$

where Δm^2 is the mass-squared difference ($m_2^2 - m_1^2$) in units of eV^2, L is the neutrino travel length in meters, and E is the neutrino energy in MeV. If the argument of the last sine function, $1.27 \times \Delta m^2 \frac{L}{E}$, is much larger than 2π, it averages out and the survival probability becomes:

$$P(\nu_e \to \nu_e) = 1 - \frac{1}{2}\sin^2 2\theta.$$

In the case of solar neutrino oscillation, the effect of matter in the Sun and the Earth must be considered. The matter effect was originally discussed by L. Wolfenstein [18] in 1978. P. Langacker, J. P. Leveille and J. Sheiman corrected a sign mistake in the Wolfensterin's paper in 1983 [19]. Then in 1985, S. P. Mikheyev and A. Y. Smirnov pointed out that the significant deficit of the event rate in Homestake, especially much less than half of the expectation, can be explained by the matter effect [20]. As you can see in the equation above, $P(\nu_e \to \nu_e)$ cannot be less than 0.5, but the matter effect can make it much less than 0.5 if $\Delta m^2 > 0$, i.e., $m_2 > m_1$. Thus, the mass ordering of m_2 and m_1 was determined by the solar neutrino observations. In 1993, global analyses had been performed [21,22] and a typical contour plot of the oscillation parameters at that time is shown in Fig. 9. The two solutions shown in the figure are called the SMA (small mixing angle) and LMA (large mixing angle) solutions for $\sin^2 2\theta \sim 10^{-2}$ and $\sin^2 2\theta \sim 0.6$, respectively.

To obtain information about neutrino oscillations, it was necessary to measure something that is independent of solar models. Possibilities were the shape of the energy spectrum and the time variation of solar neutrino event rates, such as the day/night difference. Another possibility, which is more robust, was a comparison between event rates measured with charged-current and neutral-current interactions, which are sensitive to only ν_e and all neutrino types, respectively. Regarding the shape of the energy spectrum and the day/night difference, Fig. 10 shows the neutrino survival probability as a function of energy for each solution.

Downloaded from https://academic.oup.com/ptep/article/2022/12/12B103/6543725 by Deutsches Elektronen Synchrotron user on 25 January 2023

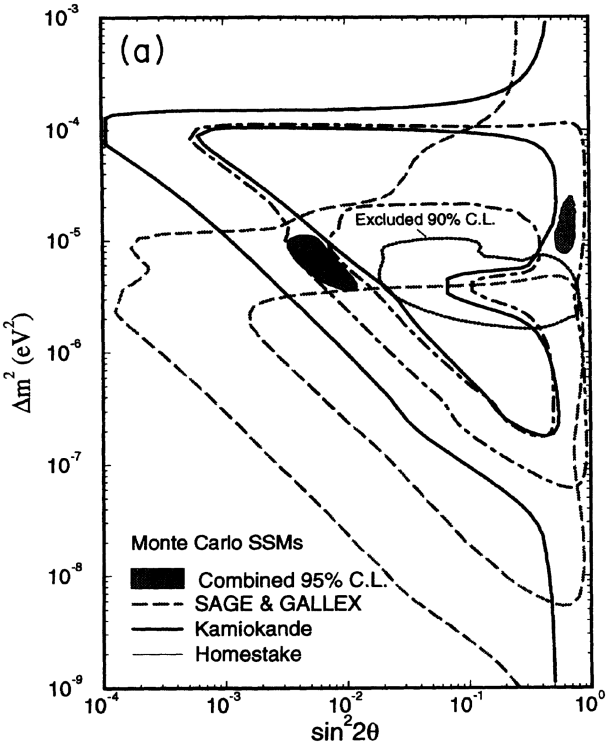

Fig. 9. Global analysis performed by Hata and Langacker in 1993 [22].

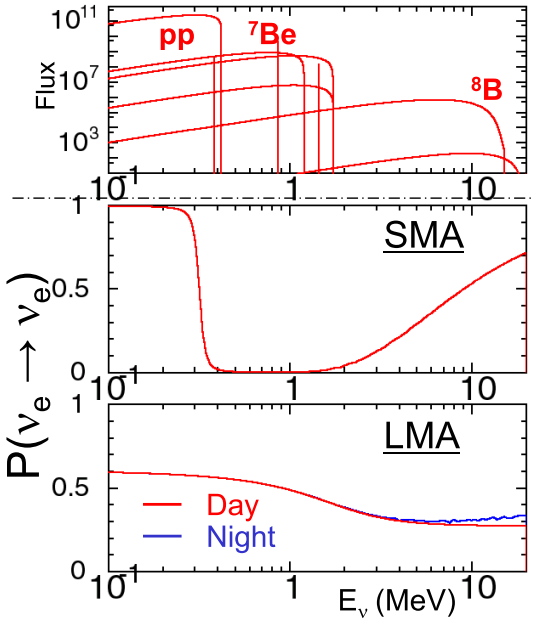

Fig. 10. Neutrino survival probability as a function of energy for typical oscillation parameters in each solution. The top plot is the predicted solar neutrino spectrum from the SSM.

Super-Kamiokande aimed to measure the energy spectrum shape distortion, which is expected for SMA, and the day/night difference, which is expected for LMA with smaller Δm^2. As will be described in Sect. 9, the first model-independent discovery of neutrino oscillations was in a comparison between a charged-current measurement by SNO (i.e., ν_e flux measurement)

Downloaded from https://academic.oup.com/ptep/article/2022/12/12B103/6543725 by Deutsches Elektronen Synchrotron user on 25 January 2023

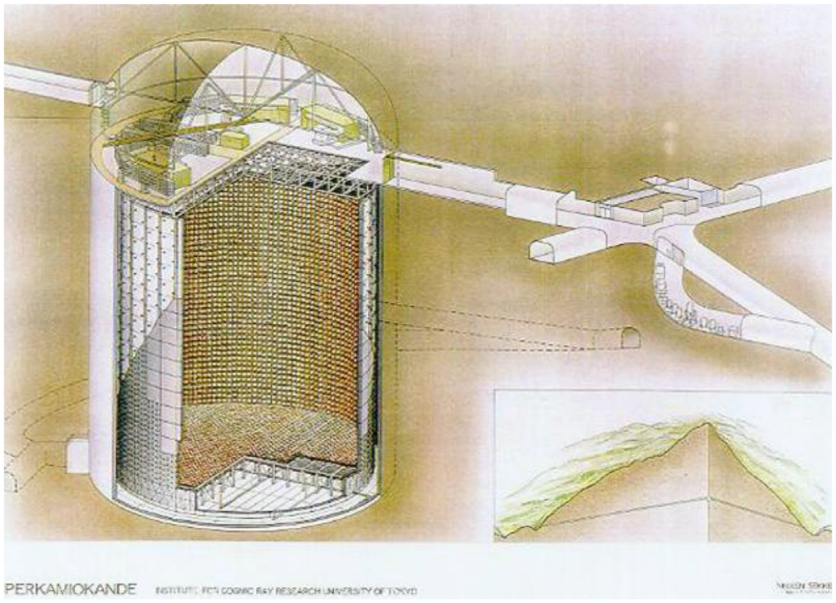

Fig. 11. Schematic view of the Super-Kamiokande detector.

and an electron-scattering measurement by Super-Kamiokande (which had contributions from ν_μ and ν_τ).

6. Super-Kamiokande

The Super-Kamiokande (SK) detector is a 50 000-ton water Cherenkov detector located 1000 m underground in the Kamioka mine in Japan. Yoji Totsuka led the detector construction and initial analyses of SK data. The detector an inner active volume (32 000 tons) viewed by 11 146 20-inch diameter photomultipliers (PMTs). The fiducial volume for the solar neutrino measurement is 22 500 tons, defined by the volume more than 2 m from the surface of the PMTs. A schematic view of the SK detector is shown in Fig. 11. SK has measured ^{8}B neutrinos using neutrino–electron scattering in the same manner as Kamiokande. The main difference between Super-Kamiokande and Kamiokande is the 30 times larger fiducial volume and increased fraction of photosensitive coverage by a factor of 2, which enabled the energy threshold to be lowered below 5 MeV.

To measure the ^{8}B solar neutrino flux energy spectrum with high precision, special care was taken at SK. The absolute energy of the detector was calibrated using an electron linear accelerator (linac) [23] installed at the detector site. The linac system could generate monoenergetic electrons and inject them at various positions in the detector. The linac system provided a very precise energy scale calibration, but it is only accurate for vertical downward-going events. To calibrate the angular dependence of the energy scale, a ^{16}N radioactive source [24] was used. ^{16}N atoms are produced by fast neutron capture by oxygen nuclei in water. Neutrons were generated by a commercially built deuteron–tritium (DT) generator that produced 10^6 14.2-MeV neutrons per pulse. The main decay mode of ^{16}N is an electron with a 4.3-MeV maximum energy coincident with a 6.1-MeV gamma ray. A setup of the DT generator was deployed in the SK tank, and it is raised by about 2 m after it emits neutrons in order to avoid shadowing the Cherenkov light. Because of the precise energy calibration by the linac and DT systems, the absolute energy scale of the SK detector was calibrated with an accuracy of 0.64%

Downloaded from https://academic.oup.com/ptep/article/2022/12/12B103/6543725 by Deutsches Elektronen Synchrotron user on 25 January 2023

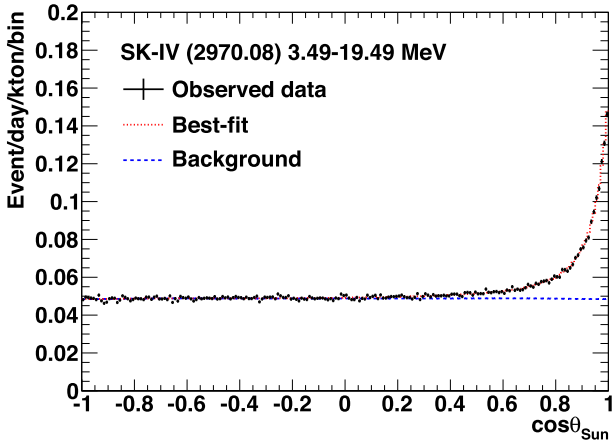

Fig. 12. Angular distribution with respect to the direction of the Sun in Super-Kamiokande phase IV [30].

Table 2. Summary of flux measurements at Super-Kamiokande.

Phase	Live-time (days)	Threshold (MeV)	Measured flux (10^6/cm^2/s)	Data/MC	# of signals (±stat. only)
SK-I	1496	4.5	$2.38\pm0.02\pm0.08$	$0.453\pm0.005^{+0.016}_{-0.014}$	$22\,443^{+227}_{-225}$
SK-II	791	6.5	$2.41\pm0.05^{+0.16}_{-0.15}$	$0.459\pm0.010\pm0.030$	7210^{+153}_{-151}
SK-III	548	4.0	$2.40\pm0.04\pm0.05$	$0.458\pm0.007\pm0.010$	8148 ± 133
SK-IV	2970	3.5	$2.33\pm0.01\pm0.03$	$0.443\pm0.003\pm0.006$	$63\,890^{+381}_{-379}$
Combined	5805	–	$2.35\pm0.01\pm0.04$	$0.447\pm0.002\pm0.008$	More than 100k events

(rms) in the first phase of the SK detector (SK-I) and was improved to 0.53% in the fourth phase.

SK-I ran for 1496 live-days from May 1996 to July 2001 [25–27]. In November 2001, a chain reaction implosion destroyed more than half of the PMTs, such that the second phase (SK-II) ran for 791 live-days from December 2002 to October 2005, using 5182 ID PMTs with 19% photocathode coverage [28]. Since SK-II the ID PMTs have been covered in fiber-reinforced plastic cases with an acrylic window to prevent similar accidents. The detector was fully reconstructed from October 2005 to July 2006 and the third phase (SK-III) ran for 548 live-days from October 2006 to August 2008 [29]. The readout electronics were replaced in September 2008 and the fourth phase (SK-IV) ran for 2970 live-days until May 2018 [30]. The SK tank was refurbished to make it leak-tight for a future upgrade (as explained later) from June 2018 to January 2019. The fifth phase (SK-V) ran from February 2019 to June 2020 with pure water. 13 tons of $Gd_2(SO_4)_3 \cdot H_2O$ was loaded into the tank water to make a 0.01%wt Gd solution from July to August in 2020 and the sixth phase (SK-VI) is running with a neutron tagging capability. Solar neutrino data analyses were performed for all SK phases and were completed by SK-IV. Figure 12 shows the angular distribution of solar neutrino candidates with respect to the direction of the Sun from SK-IV. Solar neutrino events are clearly seen above the flat background distribution. Table 2 shows live-times, energy thresholds, measured fluxes, ratios compared with a Monte Carlo simulation (in which a ^{8}B flux of 5.25×10^6/cm^2/s is assumed), the numbers of extracted signals for each SK phase, and the combined results. The

Downloaded from https://academic.oup.com/ptep/article/2022/12/12B103/6543725 by Deutsches Elektronen Synchrotron user on 25 January 2023

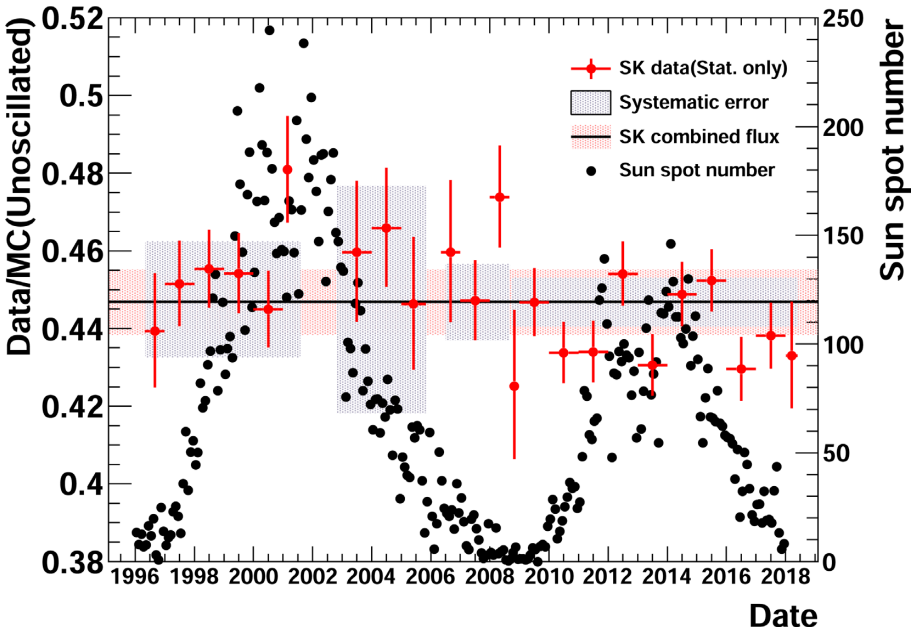

Fig. 13. Yearly plot of the ^{8}B solar neutrino flux measured by SK, shown as red points with error bars. The black dots show the number of sunspots, from Ref. [31].

energy threshold of the data analysis was 4.5 MeV (kinetic energy) in SK-I but was lowered to 3.5 MeV in SK-IV. This was possible because the radon background in the tank water was reduced by a stable laminar flow in the tank given by a precise temperature control.

In addition, the systematic error was reduced by more precise calibrations and detailed studies of the efficiencies of various cuts. When SK started data collection in 1996, solar activity was near its minimum. The SK data covered almost two solar cycles until the end of SK-IV. Figure 13 shows the measured yearly fluxes compared with the solar activity. The measured fluxes are consistent with a flat distribution within statistical and systematic errors and no correlation with the solar activity was observed.

The energy spectrum shape is important for the discussion of neutrino oscillations. Figure 14 shows energy spectra of solar neutrino signals observed in each SK phase compared with the expected spectrum without neutrino oscillations. A ^{8}B flux of $5.25 \times 10^6/\mathrm{cm}^2/\mathrm{s}$ is assumed in this figure, based on the SNO neutral-current measurement, consistent with the SSM predictions. The observed energy spectrum shapes in SK-I, II, and III are consistent with a flat oscillation probability. The SK-IV spectrum shape disfavors a flat probability with a significance of $\sim 1\sigma$, which is consistent with the shape expected from the oscillation parameters obtained by the KamLAND reactor measurement [32].

The day/night flux difference was evaluated by an asymmetry parameter (A_{DN}) defined as $\frac{(\mathrm{day}-\mathrm{night})}{\frac{1}{2}(\mathrm{day}+\mathrm{night})}$. The asymmetry parameters measured by SK-I [26], SK-II [28], SK-III [29], and SK-IV [30] were

$$A_{\mathrm{DN}}^{\mathrm{SK\text{-}I}} = -0.021 \pm 0.020(\mathrm{stat.})^{+0.013}_{-0.012}(\mathrm{sys.})$$
$$A_{\mathrm{DN}}^{\mathrm{SK\text{-}II}} = -0.063 \pm 0.042(\mathrm{stat.}) \pm 0.037(\mathrm{sys.})$$
$$A_{\mathrm{DN}}^{\mathrm{SK\text{-}III}} = -0.056 \pm 0.031(\mathrm{stat.}) \pm 0.013(\mathrm{sys.})$$
$$A_{\mathrm{DN}}^{\mathrm{SK\text{-}IV}} = -0.021 \pm 0.011(\mathrm{stat.}) \qquad (\mathrm{preliminary}).$$

Downloaded from https://academic.oup.com/ptep/article/2022/12/12B103/6543725 by Deutsches Elektronen Synchrotron user on 25 January 2023

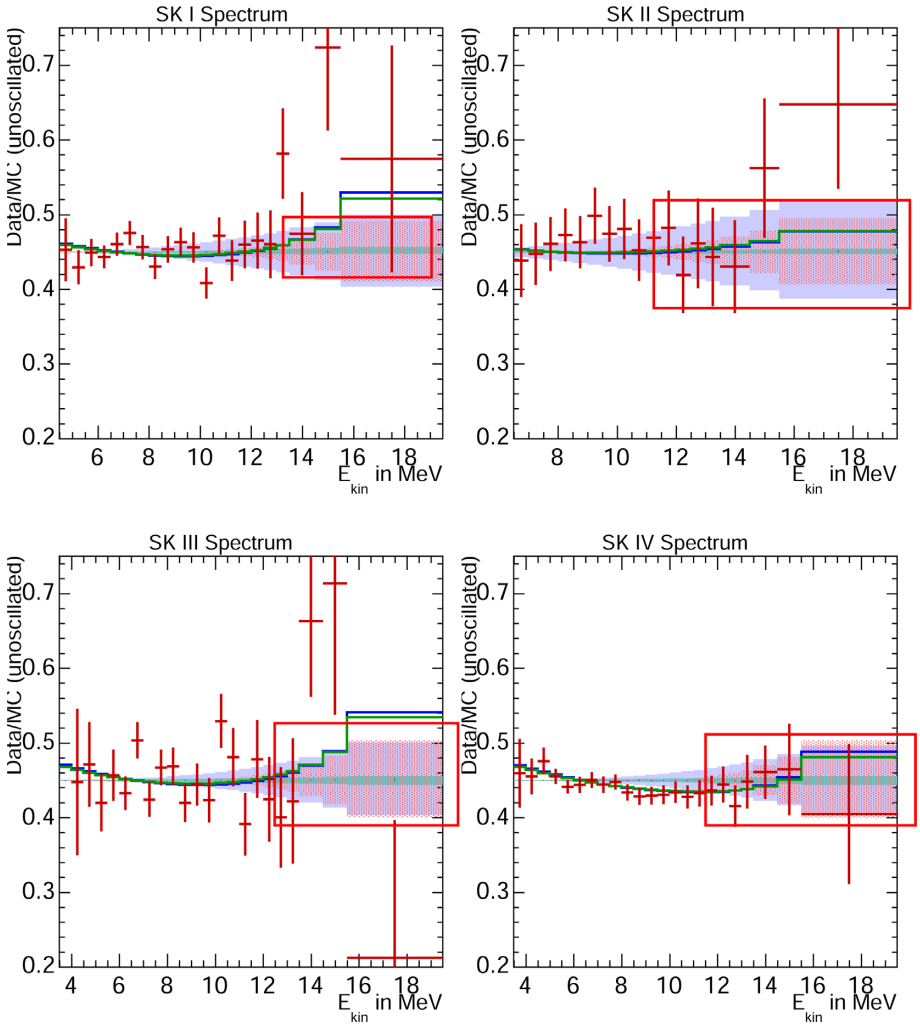

Fig. 14. Energy spectrum of the solar neutrino signal observed in each SK phase. The vertical axis is normalized by the spectrum without neutrino oscillations with a flux of $5.25 \times 10^6/\mathrm{cm}^2/\mathrm{s}$. The blue and green histograms show the expectations with neutrino oscillations with parameters from the KamLAND reactor measurement [32] and solar global analysis, respectively. The bands around the horizontal line show $\pm 1\sigma$ energy-correlated systematic errors.

Since A_{DN} depends on Δm^2, as shown by the red curve in Fig. 15, we can measure Δm^2 by A_{DN}. This is a unique method for measuring Δm^2 using solar neutrinos and is likely to be the only method for neutrinos. (Note that Δm^2 can be measured for anti-neutrinos using reactor neutrinos.) To demonstrate the accuracy of the Δm^2 measurement, A_{DN} for SK-IV is shown in Fig. 15 by black data points with statistical errors.

7. SNO

The Sudbury Neutrino Observatory (SNO) detector was a 1000-ton heavy water (D_2O) Cherenkov detector located 2090 m underground in the Creighton mine near Sudbury, Canada. It used 9456 8-inch diameter PMTs to view heavy water contained in an acrylic vessel. The SNO detector could measure the ν_e flux from ^{8}B neutrinos and the flux of all active neutrino flavors

Downloaded from https://academic.oup.com/ptep/article/2022/12/12B103/6543725 by Deutsches Elektronen Synchrotron user on 25 January 2023

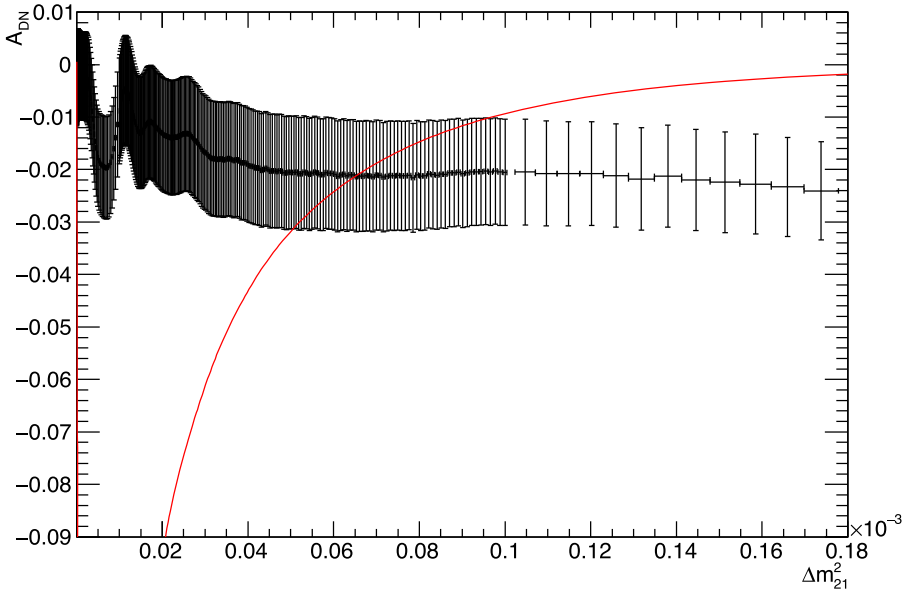

Fig. 15. Expected asymmetry from matter oscillation in the Earth as a function of Δm^2_{21} (red curve) and SK-IV data with their statistical error (black data points).

through the following interactions:

$$\begin{aligned} \nu_e + d &\rightarrow p + p + e^- \quad \text{(charged current (CC))} \\ \nu_x + d &\rightarrow p + n + \nu_x \quad \text{(neutral current (NC))} \\ \nu_x + e^- &\rightarrow \nu_x + e^- \quad \text{(electron scattering (ES))} \end{aligned}$$

where ν_x is any of ν_e, ν_μ, or ν_τ. The first phase of SNO data collection (SNO-I) was undertaken using a pure D_2O target over 306 days from November 1999 to May 2001 [33]. Free neutrons from the NC interaction were thermalized and 6.25-MeV γ rays were emitted following their capture by deuterons. The capture efficiency was about 30%. The measured fluxes were

$$\begin{aligned} \phi(^8\mathrm{B})^{\mathrm{CC}}_{\text{SNO-I}} &= 1.76 \pm 0.05(\text{stat.}) \pm 0.09(\text{sys.}) \times 10^6/\text{cm}^2/\text{s} \\ \phi(^8\mathrm{B})^{\mathrm{ES}}_{\text{SNO-I}} &= 2.39^{+0.24}_{-0.23}(\text{stat.}) \pm 0.12(\text{sys.}) \times 10^6/\text{cm}^2/\text{s} \\ \phi(^8\mathrm{B})^{\mathrm{NC}}_{\text{SNO-I}} &= 5.09^{+0.44}_{-0.43}(\text{stat.})^{+0.46}_{-0.43}(\text{sys.}) \times 10^6/\text{cm}^2/\text{s}. \end{aligned}$$

In the second phase of the SNO experiment (SNO-II), 2 tons of NaCl were added to the D_2O target to enhance the detection efficiency of the NC channel [34]. Thermalized neutrons were captured by ^{35}Cl nuclei, resulting in the emission of a γ-ray cascade with a total energy of 8.6 MeV. The CC and NC signals were statistically separated using the isotropy of the Cherenkov light pattern and each event's angle to the Sun. The forward peaked signal was due to ES and the backward distribution was due to CC interactions. NC events were isotropic with respect to the solar direction. The measured fluxes in SNO-II were

$$\begin{aligned} \phi(^8\mathrm{B})^{\mathrm{CC}}_{\text{SNO-II}} &= 1.68 \pm 0.06(\text{stat.})^{+0.08}_{-0.09}(\text{sys.}) \times 10^6/\text{cm}^2/\text{s} \\ \phi(^8\mathrm{B})^{\mathrm{ES}}_{\text{SNO-II}} &= 2.35 \pm 0.22(\text{stat.})^{+0.15}_{-0.15}(\text{sys.}) \times 10^6/\text{cm}^2/\text{s} \\ \phi(^8\mathrm{B})^{\mathrm{NC}}_{\text{SNO-II}} &= 4.94 \pm 0.21(\text{stat.})^{+0.38}_{-0.34}(\text{sys.}) \times 10^6/\text{cm}^2/\text{s}. \end{aligned}$$

In the third phase of SNO (SNO-III), ^{3}He proportional counters were deployed in the heavy water and the NC events were measured independently [35]. The NC flux measured by

Downloaded from https://academic.oup.com/ptep/article/2022/12/12B103/6543725 by Deutsches Elektronen Synchrotron user on 25 January 2023

SNO-III was

$$\phi(^8\mathrm{B})^{\mathrm{NC}}_{\mathrm{SNO\text{-}III}} = 5.54^{+0.33}_{-0.31}(\mathrm{stat.})^{+0.36}_{-0.34}(\mathrm{sys.}) \times 10^6/\mathrm{cm}^2/\mathrm{s}.$$

The SNO group performed a combined analysis [36] of all three phases and the obtained result was

$$\phi(^8\mathrm{B})^{\mathrm{NC}}_{\mathrm{SNO\ combined}} = 5.25 \pm 0.16(\mathrm{stat.})^{+0.11}_{-0.13}(\mathrm{sys.}) \times 10^6/\mathrm{cm}^2/\mathrm{s}\ .$$

Compared with the ^{8}B flux value in Table 1, the observed ^{8}B flux with NC by SNO agrees well with the prediction within the errors. Combining the statistical and systematic errors, the total error of the flux observed by SNO is 3.8%, which is better than that of the SSM prediction by a factor of 3. Therefore, the SNO value was used to make plots of SK in the previous section and will be used in the discussion of the global oscillation analysis in Sect. 9.

8. Borexino

Borexino is a liquid scintillator detector with an active mass of 278 tons of pseudocumene located in the Gran Sasso Laboratory. Scintillation light is detected via 2212 8-inch PMTs uniformly distributed on the inner surface of the detector. Because of the high light yield of a liquid scintillator compared with Cherenkov light, Borexino is sensitive to sub-MeV solar neutrinos. The first ^{7}Be solar neutrino measurement was reported in Ref. [37], based on 192 days of data taken from May 2007 to April 2008. The 0.862-MeV monoenergetic ^{7}Be neutrinos were detected by neutrino–electron scattering. The energy spectrum of observed events was deconvoluted using the expected shape of the recoil electrons and possible background sources. Thus, the extracted ^{7}Be neutrino event rate was

$$49 \pm 3(\mathrm{stat.}) \pm 4(\mathrm{sys.})\ \mathrm{counts}/(\mathrm{day} \cdot 100\,\mathrm{ton}),$$

while the expected event rate from the SSM was 74 ± 4 counts/(day $\cdot$ 100 ton). The deficit of the observed ^{7}Be neutrino event rate is consistent with the expectation based on neutrino oscillations. Borexino also succeeded in observing *pep*, *pp*, and CNO solar neutrinos, reported in Refs. [38], [39], and [40], respectively. The Borexino group corrected the effect of neutrino oscillations and obtained fluxes of *pp*, ^{7}Be, *pep*, and CNO neutrinos from the second phase of Borexino as [40,41]

$$\begin{aligned}
\phi(pp)^{\mathrm{Osc.corrected}}_{\mathrm{Borexino}} &= 6.1 \pm 0.5(\mathrm{stat.})^{+0.3}_{-0.5}(\mathrm{sys.}) \times 10^{10}/\mathrm{cm}^2/\mathrm{s} \\
\phi(^7\mathrm{Be})^{\mathrm{Osc.corrected}}_{\mathrm{Borexino}} &= 4.99 \pm 0.11(\mathrm{stat.})^{+0.06}_{-0.08}(\mathrm{sys.}) \times 10^{9}/\mathrm{cm}^2/\mathrm{s} \\
\phi(pep(HZ/LZ))^{\mathrm{Osc.corrected}}_{\mathrm{Borexino}} &= 1.27/1.39 \pm 0.19(\mathrm{stat.})^{+0.08}_{-0.12/-0.13}(\mathrm{sys.}) \times 10^{8}/\mathrm{cm}^2/\mathrm{s} \\
\phi(\mathrm{CNO})^{\mathrm{Osc.corrected}}_{\mathrm{Borexino}} &= 7.0^{+3.0}_{-2.0}(\mathrm{sys.}) \times 10^{8}/\mathrm{cm}^2/\mathrm{s}.
\end{aligned}$$

These fluxes are compared with the SSM predictions in Table 1 and are consistent with each other within the experimental errors.

9. Solar neutrino oscillations

Precise solar neutrino measurements have shown that the solar neutrino problem is due to neutrino oscillations. In this section, a brief history of and the latest results for solar neutrino oscillations are discussed.

Downloaded from https://academic.oup.com/ptep/article/2022/12/12B103/6543725 by Deutsches Elektronen Synchrotron user on 25 January 2023

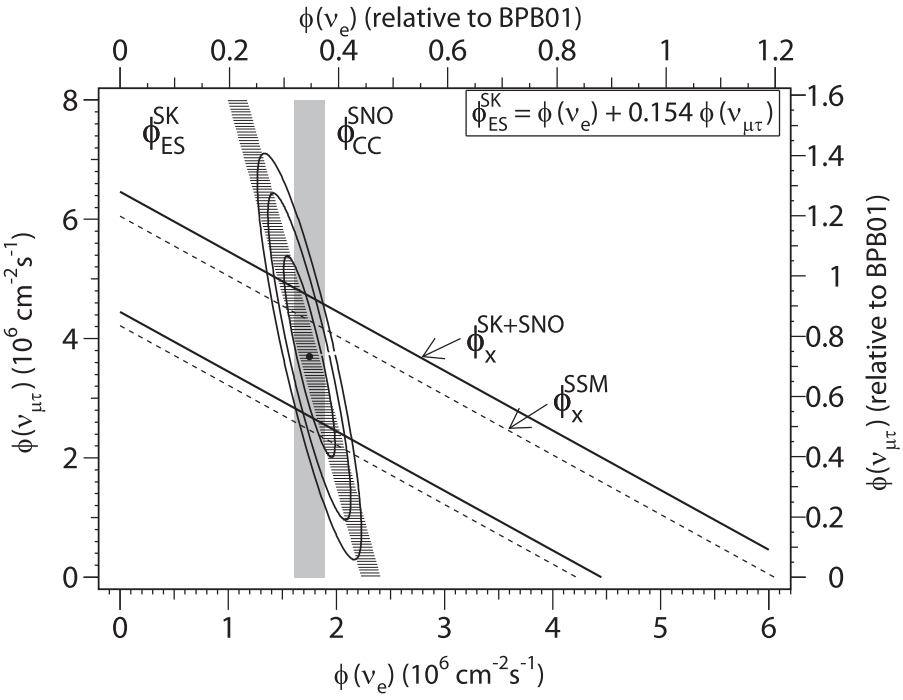

Fig. 16. ν_e flux and $\nu_{\mu/\tau}$ flux contour obtained from the results of SK and SNO in 2001 [42]. Each band shows the $\pm 1\sigma$ range of each measurement.

9.1 *Evidence of solar neutrino oscillations*

In March 2001, the SK Collaboration released results of the precise measurement of the ^{8}B flux using 1258 days of SK data [25]. SK measured ^{8}B solar neutrinos using neutrino–electron scattering (ES), in which ν_μ and ν_τ contribute in addition to ν_e because the cross section of $\nu_{\nu/\tau}e^-$ scattering is about 1/(6–7) of that for $\nu_e e^-$ scattering. In June 2001, the SNO Collaboration released the first result of the charged-current (CC), i.e., ν_e, measurement, including the plot in Fig. 16, which demonstrated that $\nu_{\mu/\tau}$ exist with more than 3σ significance [42]. That was the first direct evidence for solar neutrino oscillations. The SNO Collaboration published NC measurements, the results of which are described above in Sect. 7. The SK Collaboration provided further data for analysis and improved the accuracy of the ES measurement. The plot in Fig. 17 uses the latest data from SK and SNO, including NC data, showing that the significance of $\nu_{\mu/\tau}$ had been greatly improved. The measurements of SK and SNO are consistent with each other.

9.2 *Determination of oscillation parameters*

In the three-flavor neutrino framework, the relation between the mass and interaction eigenstates is described by

$$\begin{pmatrix} \nu_e \\ \nu_\mu \\ \nu_\tau \end{pmatrix} = \begin{pmatrix} U_{e1} & U_{e2} & U_{e3} \\ U_{\mu 1} & U_{\mu 2} & U_{\mu 3} \\ U_{\tau 1} & U_{\tau 2} & U_{\tau 3} \end{pmatrix} \begin{pmatrix} \nu_1 \\ \nu_2 \\ \nu_3 \end{pmatrix}.$$

Downloaded from https://academic.oup.com/ptep/article/2022/12/12B103/6543725 by Deutsches Elektronen Synchrotron user on 25 January 2023

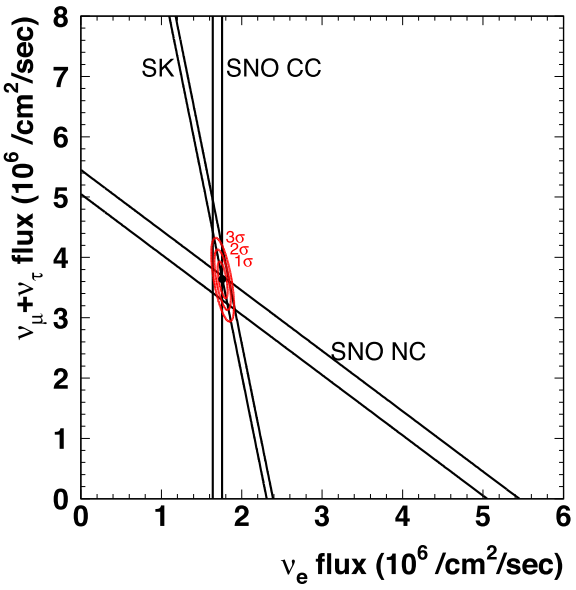

Fig. 17. Latest ν_e flux and $\nu_{\mu/\tau}$ flux contour obtained from the results of SK [30] and SNO [33–35,36]. Each band shows the $\pm 1\sigma$ range for each measurement.

The unitary matrix U is the Pontecorvo–Maki–Nakagawa–Sakata (PMNS) matrix and can be decomposed into three angles and a phase:

$$U = \begin{pmatrix} 1 & 0 & 0 \\ 0 & c_{23} & s_{23} \\ 0 & -s_{23} & c_{23} \end{pmatrix} \begin{pmatrix} c_{13} & 0 & s_{13}e^{-i\delta} \\ 0 & 1 & 0 \\ -s_{13}e^{i\delta} & 0 & c_{13} \end{pmatrix} \begin{pmatrix} c_{21} & s_{12} & 0 \\ -s_{12} & c_{12} & 0 \\ 0 & 0 & 1 \end{pmatrix}$$
$$= \begin{pmatrix} c_{12}c_{13} & s_{12}c_{13} & s_{13}e^{-i\delta} \\ -s_{12}c_{23} - c_{12}s_{23}s_{13}e^{i\delta} & c_{12}c_{23} - s_{12}s_{23}s_{13}e^{i\delta} & s_{23}c_{13} \\ s_{12}s_{23} - c_{12}c_{23}s_{13}e^{i\delta} & -c_{12}s_{23} - s_{12}c_{23}s_{13}e^{i\delta} & c_{23}c_{13} \end{pmatrix},$$

where $c_{ij} \equiv \cos\theta_{ij}$ and $s_{ij} \equiv \sin\theta_{ij}$. In addition, the mass-squared differences ($\Delta m^2_{ij} (= m^2_i - m^2_j)$) Δm^2_{21} and Δm^2_{32} affect the oscillations. In the solar neutrino oscillation analysis, the oscillation probability can be calculated using three parameters, θ_{12}, θ_{13}, and Δm^2_{21}, because $|\Delta m^2_{21}| \ll |\Delta m^2_{32}|$.

The green contours in Fig. 18 show the allowed region of the oscillation parameters, θ_{12} and Δm^2_{21}, obtained from the SK data. The total flux of ^{8}B is constrained by the SNO NC flux measurement ($(5.25 \pm 0.20) \times 10^6$/cm^2/s). The θ_{13} value is constrained to $\sin^2(\theta_{13}) = 0.0219 \pm 0.0014$ by the short-baseline reactor neutrino measurements [43–45]. The LMA solution is more than 4σ-level more significant than the other solutions and the result is consistent with the long-baseline reactor measurement by KamLAND [32] shown by the blue contours in the figure. The same plot on a linear scale is shown in Fig. 19. Figure 20 shows the allowed region obtained by combining the SK and SNO data.

10. Conclusion and future prospects

The solar neutrino problem suggested by the Homestake experiment has led to some very interesting outcomes. Owing to the insight of Prof. Koshiba, the solar neutrino problem was confirmed by a water Cherenkov detector, Kamiokande. The water Cherenkov technique was

Downloaded from https://academic.oup.com/ptep/article/2022/12/12B103/6543725 by Deutsches Elektronen Synchrotron user on 25 January 2023

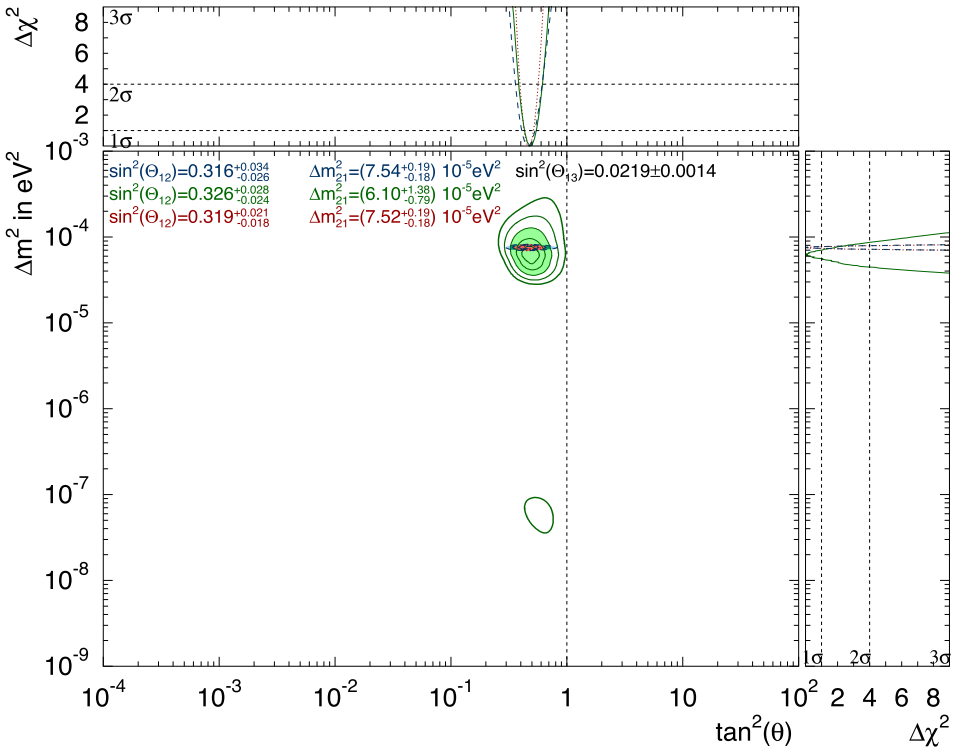

Fig. 18. Oscillation parameters obtained from SK data [30] compared with the KamLAND reactor data [32]. The green contours show the allowed region of θ_{12} and Δm^2_{21} obtained from the SK data with the ^{8}B flux constrained by the SNO NC value($(5.25 \pm 0.20) \times 10^6/\mathrm{cm}^2/\mathrm{s}$). The lines show 1, 2, 3, 4, and 5σ significance from inside to outside. The light-blue filled area shows the KamLAND reactor contour with 3σ and the brown filled area shows the SK and KamLAND combined result with 3σ.

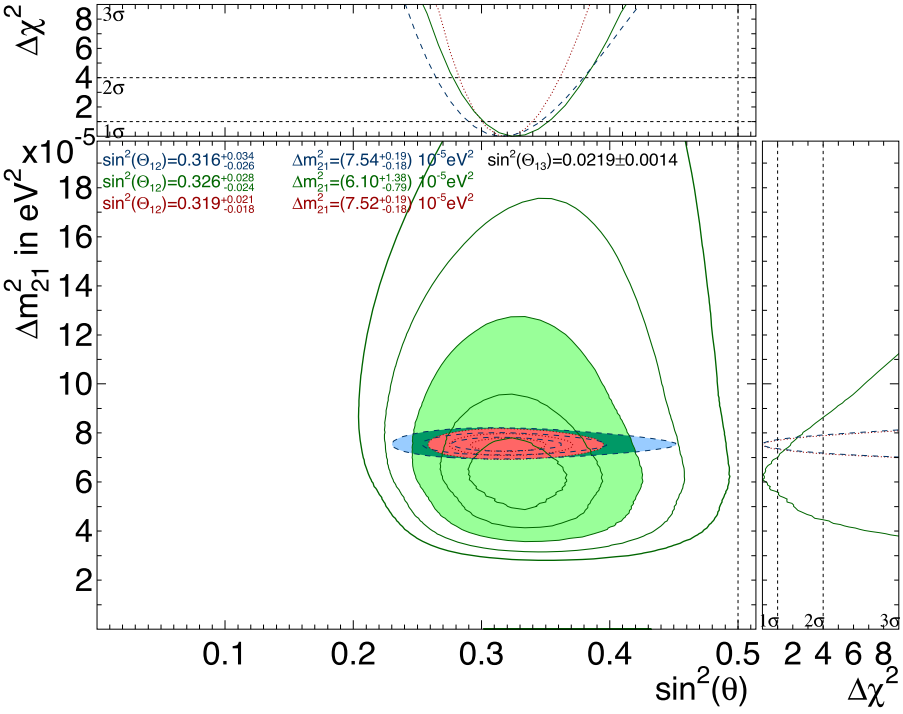

Fig. 19. As for Fig. 18 but with a linear scale on the vertical axis. The green, light-blue, and brown regions show contours of SK, KamLAND, and the combination of SK and KamLAND, respectively.

Downloaded from https://academic.oup.com/ptep/article/2022/12/12B103/6543725 by Deutsches Elektronen Synchrotron user on 25 January 2023

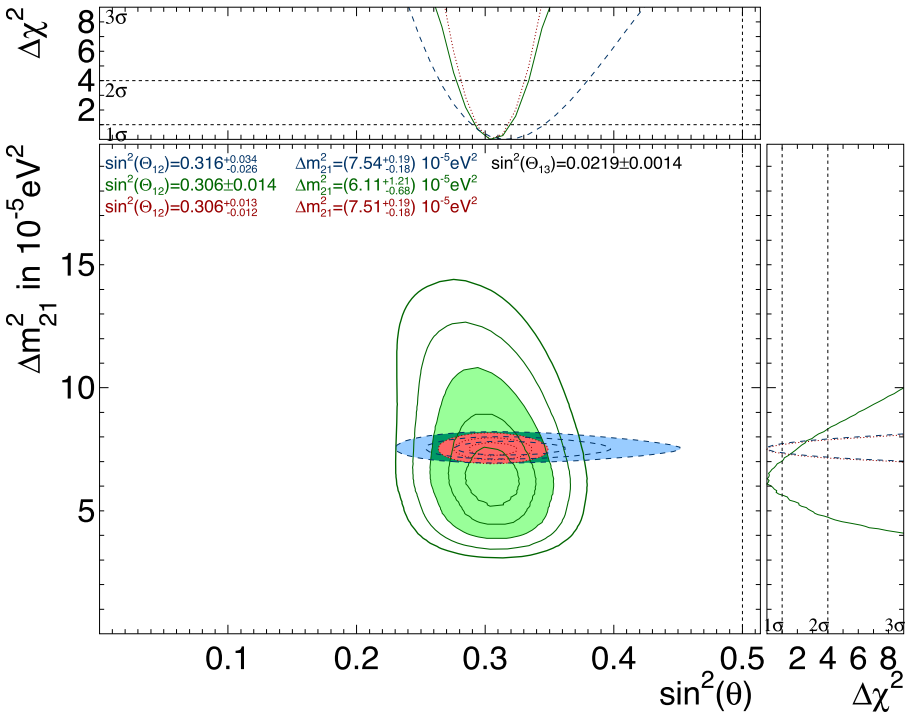

Fig. 20. Oscillation parameters obtained from SK and SNO data compared with the KamLAND reactor data [32]. The green contours show the allowed region of θ_{12} and Δm^2_{21} obtained from the SK and SNO data. The lines show the 1, 2, 3, 4, and 5σ significance from inside to outside. The light-blue filled area shows the KamLAND reactor contour with 3σ, and the brown filled area shows the SK, SNO, and KamLAND combined contour with 3σ.

adopted in Super-Kamiokande and SNO and precise measurements of the ^{8}B solar neutrino flux were conducted. In particular, the flux difference between the neutral-current and charged-current methods, which are sensitive to all types of neutrinos and only to ν_e, respectively, provided smoking-gun evidence of neutrino oscillations. All the results from solar neutrino experiments (Homestake, Kamiokande, SAGE, GALLEX/GNO, Super-Kamiokande, SNO, and Borexino) can be shown to be consistent with the expectations from the standard solar model with neutrino oscillations. This is a great accomplishment that would not have been possible without the insight of Prof. Koshiba.

Is this the end of the story for solar neutrinos? I do not think so. The measurements of the ^{8}B spectrum shape and the day/night difference are not yet precise enough to allow a proper discussion of neutrino oscillations. Borexino succeeded in observing CNO neutrinos but without sufficient precision to discuss the low- and high-metallicity models. The most abundant solar neutrino source is *pp* neutrinos, the flux of which the SSM predicts with an accuracy of ∼1%. However, the experimental results are not yet this precise. Something interesting might still be hidden in solar neutrinos.

Acknowledgements

The author gratefully acknowledges the cooperation of the Super-Kamiokande collaborators in providing the main contents of the SK results and oscillation analyses. The author also wishes to thank the proposers of this special issue (Profs. Mitsuaki Nozaki and Masashi Yokoyama) for giving him the opportunity to write this article.

Downloaded from https://academic.oup.com/ptep/article/2022/12/12B103/6543725 by Deutsches Elektronen Synchrotron user on 25 January 2023

Funding

Open Access funding: SCOAP[3].

References

1 J. N. Bahcall, M. H. Pinsonneault, and S. Basu, Astrophys. J. **555**, 990 (2001).
2 J. N. Bahcall and M. H. Pinsonneault, Phys. Rev. Lett. **92**, 121301 (2004).
3 N. Vinyoles, A. M. Serenelli, F. L. Villante, S. Basu, J. Bergström, M. C. Gonzalez-Garcia, M. Maltoni, C. Peña-Garay, and N. Song, Astrophys. J. **835**, 202 (2017).
4 N. Grevesse and A. J. Sauval, Space Sci. Rev. **85**, 161 (1998).
5 M. Asplund, N. Grevesse, A. J. Sauval, and P. Scott, Ann. Rev. Astron. Astrophys. **47**, 481 (2009).
6 B. T. Cleveland et al. Astrophys. J. **496**, 505 (1998).
7 B. Pontecorvo, Chalk River Report PD-205 (1946).
8 H. Georgi and S. L. Glashow, Phys. Rev. Lett. **32**, 438 (1974).
9 K. S. Hirata et al. [Kamiokande-II Collaboration], Phys. Rev. Lett. **63**, 16 (1989).
10 Y. Fukuda et al. [Kamiokande Collaboration], Phys. Rev. Lett. **77**, 1683 (1996).
11 Dzh. N. Abdurashitov et al. Phys. Lett. B **328**, 234 (1994).
12 V. N. Gavrin et al. [SAGE Collaboration], Nucl. Phys. B Proc. Suppl. **91**, 36 (2001).
13 J. N. Abdurashitov et al. Phys. Rev. C **80**, 015807 (2009).
14 P. Anselmann et al. [GALLEX Collaboration], Phys. Lett. B **327**, 377 (1994).
15 P. Anselmann et al. [GALLEX Collaboration], Phys. Lett. B **357**, 237 (1995).
16 W. Hampel et al. [GALLEX Collaboration], Phys. Lett. B **388**, 384 (1996).
17 M. Altmann et al. [GNO Collaboration], Phys. Lett. B **616**, 174 (2005).
18 L. Wolfenstein, Phys. Rev. D **17**, 2369 (1978).
19 P. Langacker, J. P. Leveille, and J. Sheiman, Phys. Rev. D **27**, 1228 (1983).
20 S. P. Mikheyev and A. Y. Smirnov, Sov. J. Nucl. Phys. **42**, 913 (1985).
21 P. I. Krastev and S. T. Petcov, Phys. Lett. B **299**, 99 (1993).
22 N. Hata and P. Langacker, Phys. Rev. D **50**, 632 (1994) [arXiv:hep-ph/9311214] [Search inSPIRE].
23 M. Nakahata et al. [Super-Kamiokande Collaboration], Nucl. Instrum. Meth. A **421**, 113 (1999).
24 E. Blaufuss et al. [Super-Kamiokande Collaboration], Nucl. Instrum. Meth. A **458**, 638 (2001).
25 S. Fukuda et al. [Super-Kamiokande Collaboration], Phys. Rev. Lett. **86**, 5651 (2001).
26 S. Fukuda et al. [Super-Kamiokande Collaboration], Phys. Lett. B **539**, 179 (2002).
27 J. Hosaka et al. [Super-Kamiokande Collaboration], Phys. Rev. D **73**, 112001 (2006).
28 J. P. Cravens et al. [Super-Kamiokande Collaboration], Phys. Rev. D **78**, 032002 (2008).
29 K. Abe et al. [Super-Kamiokande Collaboration], Phys. Rev. D **83**, 052010 (2011).
30 Y. Nakajima et al. [Super-Kamiokande Collaboration]; Presentation at The XXIX International Conference on Neutrino Physics and Astrophysics (Neutrino 2020).
31 WDC-SILSO, Royal Observatory of Belgium, Brussels. http://www.sidc.be/silso/datafiles.
32 S. Abe et al. [KamLAND Collaboration], Phys. Rev. Lett. **100**, 221803 (2008).
33 Q. R. Ahmad et al. [SNO Collaboration], Phys. Rev. Lett. **89**, 011301 (2002).
34 B. Aharmim et al. [SNO Collaboration], Phys. Rev. C **72**, 055502 (2005).
35 B. Aharmim et al. [SNO Collaboration], Phys. Rev. Lett. **101**, 111301 (2008).
36 B. Aharmim et al. [SNO Collaboration], Phys. Rev. C **88**, 025501 (2013).
37 C. Arpesella et al. [Borexino Collaboration], Phys. Rev. Lett. **101**, 091302 (2008).
38 G. Bellini et al. [Borexino Collaboration], Phys. Rev. Lett. **108**, 051302 (2012).
39 G. Bellini et al. [Borexino Collaboration], Nature **512**, 383 (2014).
40 M. Agostini et al. [Borexino Collaboration], Nature **587**, 577 (2020).
41 M. Agostini et al. [Borexino Collaboration], Phys. Rev. D **100**, 082004 (2019).
42 Q. R. Ahmad et al. [SNO Collaboration], Phys. Rev. Lett. **87**, 071301 (2001).
43 F. P. An et al. [Daya Bay Collaboration], Chin. Phys. C **37**, 011001 (2013).
44 J. K. Ahn et al., Phys. Rev. Lett. **108**, 191802 (2012).
45 Y. Abe et al., Phys. Rev. D **86**, 052008 (2012).

Downloaded from https://academic.oup.com/ptep/article/2022/12/12B103/6543725 by Deutsches Elektronen Synchrotron user on 25 January 2023